Article

Future Landslide Characteristic Assessment Using Ensemble Climate Change Scenarios: A Case Study in Taiwan

Yung-Ming Chen [1], Chi-Wen Chen [2,3,*], Yi-Chiung Chao [1], Yu-Shiang Tung [1], Jun-Jih Liou [1], Hsin-Chi Li [1] and Chao-Tzuen Cheng [1]

[1] National Science and Technology Center for Disaster Reduction, No. 200, Sec. 3, Beixin Road, Xindian District, New Taipei City 23143, Taiwan; ymchen@ncdr.nat.gov.tw (Y.-M.C.); ycchao@ncdr.nat.gov.tw (Y.-C.C.); ystung@ncdr.nat.gov.tw (Y.-S.T.); jjliou@ncdr.nat.gov.tw (J.-J.L.); hsinchi@ncdr.nat.gov.tw (H.-C.L.); ctcheng@ncdr.nat.gov.tw (C.-T.C.)
[2] Center for Spatial Information Science, The University of Tokyo, 5-1-5 Kashiwanoha Kashiwa, Chiba 277-8568, Japan
[3] National Research Institute for Earth Science and Disaster Resilience, Tsukuba, Ibaraki 305-0006, Japan
* Correspondence: kevin4919@gmail.com; Tel.: +81-29-863-7579; Fax: +81-29-854-0629

check for updates

Abstract: Affected by climate change owing to global warming, the frequency of extreme rainfall events has gradually increased in recent years. Many studies have analyzed the impacts of climate change in various fields. However, uncertainty about the scenarios they used is still an important issue. This study used two and four multi-scenarios at the base period (1979–2003) and the end of the 21st century (2075–2099) to collect the top-ranking typhoons and analyze the rainfall conditions of these typhoons in two catchments in northern Taiwan. The landslide-area characteristics caused by these typhoons were estimated using empirical relationships, with rainfall conditions established by a previous study. In addition to counting landslide-area characteristics caused by the typhoons of each single scenario, we also used the ensemble method to combine all scenarios to calculate landslide-area characteristic statistics. Comparing the statistical results of each single scenario and the ensembles, we found that the ensemble method minimized the uncertainty and identified the possible most severe case from the simulation. We further separated typhoons into the top 5%, 5%–10%, and 10%–15% to confirm possible changes in landslide-area characteristics under climate change. We noticed that the uncertainty of the base period and the end of the 21st century almost overlapped if only a single scenario was used. In contrast, the ensemble approach successfully distinguished the differences in both the average values of landslide-area characteristics and the 95% confidence intervals. The ensemble results indicated that the landslide magnitude triggered by medium- and high-level typhoons (top 5%–15%) will increase by 24%–29% and 125%–200% under climate change in the Shihmen Reservoir catchment and the Xindian River catchment, respectively, while landslides triggered by extreme-level typhoons (top 5%) will increase by 8% and 77%, respectively. Still, the uncertainty of landslide-area characteristics caused by extreme typhoon events is slightly high, indicating that we need to include more possible scenarios in future work.

Keywords: climate change; dynamical downscaling; landslide; typhoon; empirical relationship; sea surface temperature; ensemble; scenario; uncertainty

1. Introduction

The Intergovernmental Panel on Climate Change (IPCC) has reported that global warming will lead to climate change, which will cause sea levels to rise and climate variability [1,2]. The latter

includes the frequency, extension, and intensity of drought and extreme rainfall events, which may increase significantly. As a result of the increasing frequency and intensity of extreme rainfall events, the prevention and control of landslide disasters will face greater challenges worldwide [3,4]. Many factors affect the occurrence of landslides, such as topographic and geologic conditions, land use, and precipitation [5,6]. However, in the case of small changes and almost unpredictable predisposing factors, rainfall is one of the important triggering factors of changing landslide characteristics under climate change [7–9].

Many studies have explored the potential impact of different climate change scenarios on landslide disasters [10,11]. Jakob and Lambert [9] pointed out that the number of extreme rainfall events that will trigger landslides in Howe Sound, Canada, will increase by as much as 28% by 2071–2100. Chiang and Chang [12] evaluated the impact of climate change on the high landslide susceptibility area in the Baishi River catchment, Taiwan, and indicated that from 2010 to 2099, the high landslide susceptibility area would increase by about 12.8% in the catchment. Note that for the temporal downscaling of precipitation data of those studies, the long-term meteorological data (monthly) were directly converted into short-term data (24 hours) in a statistical approach. This kind of method for temporal downscaling increases the uncertainty in the assessment of climate change impacts [13–15]. Chen et al. [16] used dynamically downscaled rainfall data to estimate landslide-area characteristics caused by typhoon events at the base period (1979–2003) and the end of the 21st century (2075–2099) in two catchments in northern Taiwan. However, only one scenario was simulated to obtain dynamically downscaled rainfall data, that is, the impacts of climate change remain uncertain.

Landslide disasters in Taiwan are a topic of great concern to the public today [17–19]. When typhoons come, they often cause landslides in mountainous areas, resulting in huge losses of public facilities, property, and life. In the current changing environment, both the probability of the occurrence of a strong typhoon and the rainfall intensity during a typhoon event will increase [20–22]. According to a climate change report from Taiwan, the frequency of extreme rainfall events has also increased in the past 20 years in Taiwan [23]. Under the impact of climate change, extreme rainfall events will become more frequent, and the possibility of landslides in the upstream area will increase significantly. Therefore, effectively assessing the impact of climate change on future landslide characteristics and minimizing the uncertainty of the assessment are essential and important issues. The objectives of this study were to use the dynamically downscaled rainfall data of all the scenarios currently available in Taiwan to select top-ranking typhoons for each scenario, and to estimate landslide-area characteristics according to the rainfall conditions of each typhoon event for two catchments in northern Taiwan. All scenarios were combined using the ensemble approach, and the uncertainty of landslide-area characteristic evaluation between each single scenario and the ensembles is discussed. Finally, we used the ensemble method to estimate how landslide-area characteristics of the two catchments will be affected under climate change.

2. Climate Change Scenarios

2.1. Base Period (1979–2003)

Two scenarios for the base period are widely used in Taiwan. The first is the scenario proposed by the IPCC in the Fourth Assessment Report, 2007 (AR4), which is the Coupled Model Intercomparison Project Phase 3 (CMIP3) model under the Special Report on Emission Scenarios (SRES) A1B scenario [1]. We call this scenario "m00". The second is the scenario proposed by the IPCC in the Fifth Assessment Report, 2013 (AR5), which is the Coupled Model Intercomparison Project Phase 5 (CMIP5) model under the representative concentration pathways 8.5 (RCP8.5) [2]. This scenario is called "m01". The RCP8.5 is a hypothetical scenario that no country in the world has reduced greenhouse gas emissions. This scenario is a relatively worst-case emission scenario that can be used for a severe scenario estimation and for the conservative adjustment. In terms of rainfall, the seasonal and annual rainfall change rate under climate change of the A1B scenario is similar to those of the RCP8.5.

They have the climatic characteristics that rainfall increases during the wet season and decreases during the dry season.

2.2. End of 21st Century (2075–2099)

The targeted projection window for the future climate is the last quarter of the 21st century. The model is computed from future projections by CMIP5 models under the RCP8.5. Mizuta et al. [24] classified 28 CMIP5 models into three clusters by a cluster analysis of annual-mean tropical sea surface temperature (SST) change patterns. The classified SST change patterns are featured by the zonal gradient of the change in the equatorial Pacific and interhemispheric contrast of the warming. Precipitation and atmospheric circulation responses are composited for the clusters. Based on Mizuta et al. [24], we developed four scenarios for the future SSTs. One is the multi-model ensemble mean of SST computed from all models (average value of all models), which we call "c0". The other three patterns were created using a cluster analysis, in which normalized tropical SST anomalies derived from the 28 models were grouped to avoid subjective selection of a single model, which we call clusters 1, 2, and 3, denoted as "c1", "c2", and "c3" [24]. The procedure of clustering is based on a single-linkage method, where the minimum distance between two models or groups is gradually added [25]. When the last three groups are obtained, the clustering process is terminated. The detailed classification method was described by Mizuta et al. [24], and the average SSTs in different seasons under these scenarios are shown in Figure 1.
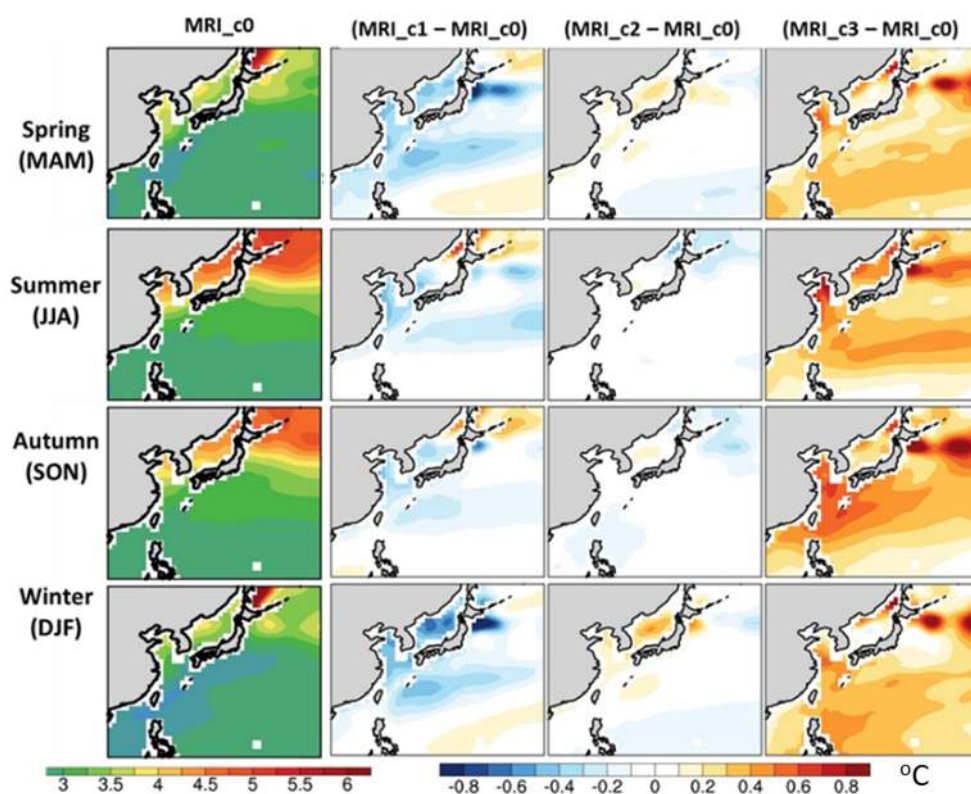

Figure 1. The average sea surface temperatures (SSTs) in different seasons under the c0 scenario and differences between other scenarios and c0. MAM: March, April, and May; JJA: June, July, and August; SON: September, October, and November; DJF: December, January, and February.

3. Data and Methods

3.1. Climate Change Data in Taiwan

The general circulation model (GCM) for climate estimation and simulation typically has a resolution of 100–200 km. It is difficult to identify the structure of a typhoon with a radius of less

than several hundred kilometers. Due to the low spatial resolution of the model, it is impossible to reasonably simulate extreme weather systems with physical models, and it is impossible to estimate extreme weather under climate change. [26,27]. Therefore, this study used a climate projection modeled from the high-resolution (approximately 20-km horizontal resolution) atmospheric general circulation model (AGCM) developed by the Meteorological Research Institute (MRI) of the Japan Meteorological Agency (JMA) [28]. The model incorporating the climate change scenario of A1B and RCP8.5 in CMIP 3/5 [24] is called MRI-AGCM. In addition, for the simulation of the end of the 21st century, the low boundary can be driven by different SSTs mentioned in the previous section on the c0, c1, c2, and c3 scenarios. This model has been verified by simulation of typhoon generation [29,30]. However, the horizontal resolution of 20 km may not necessarily reflect the intensity of precipitation caused by the terrain effect in Taiwan. Therefore, the Weather Research and Forecasting Model (WRF), proposed by the US National Center for Atmospheric Research (NCAR), was used to dynamically downscale the MRI–AGCM data to obtain more realistic rainfall data in Taiwan with a spatiotemporal resolution of 5 km per hour. According to the downscaled rainfall data, during the base period, there are 82 and 84 typhoons in the m00 and m01 scenarios, but 45, 23, 55, and 46 typhoons in the c0, c1, c2, and c3 scenarios, respectively, in the last quarter of the 21st century (Table 1).

Table 1. The total number of typhoons and number of top 5%, 10%, and 15% typhoons in each climate change scenario and ensemble.

Scenario	Total Number of Typhoons	Number of Top Typhoons		
		5%	10%	15%
m00	82	4	8	12
m01	84	4	8	12
Ensemble	166	8	16	24
c0	45	2	5	7
c1	23	1	2	3
c2	55	3	6	9
c3	46	2	5	7
Ensemble	169	8	17	25

3.2. Calculation of Landslide-Area Characteristics

Chen et al. [16] established the relationship between rainfall conditions and landslide-area characteristics for two catchments in northern Taiwan, the Shihmen Reservoir catchment and the Xindian River catchment (Figure 2). They found that the landslide-area characteristics in the Shihmen Reservoir catchment are highly correlated with cumulative rainfall during a typhoon event. On the other hand, the landslide-area characteristics in the Xindian River catchment are highly correlated with peak rainfall intensity during a typhoon event. The empirical relationships are as follows:

For the Shihmen Reservoir catchment:

$$A_T = 4697.3 \times E + 737287 \tag{1}$$

$$L = 0.0006 \times E + 0.0974 \tag{2}$$

$$A_M = 921.69 \times E - 141948 \tag{3}$$

$$N = 0.6969 \times E + 71.532 \tag{4}$$

For the Xindian River catchment:

$$A_T = 23764 \times I_P - 547585 \tag{5}$$

$$L = 0.0049 \times I_P - 0.1119 \tag{6}$$

$$A_{\mathrm{M}} = 3924.4 \times I_{\mathrm{p}} - 89062 \tag{7}$$

$$N = 6.0251 \times I_{\mathrm{p}} - 137.23 \tag{8}$$

where A_{T} is total landslide area (m^2), L is landslide-area ratio (%), A_{M} is maximum landslide area (m^2), N is number of landslides, E is cumulative rainfall (mm), and I_{p} is peak rainfall intensity (mm/h). Although the empirical approach is an effective method to identify landslide-area characteristics, it is evaluated by the interpolation or extrapolation. According to these formulas, when rainfall conditions are weak, unreasonable negative values of landslide-area characteristics may be calculated, and it can be considered that the rainfall conditions cannot trigger landslides.
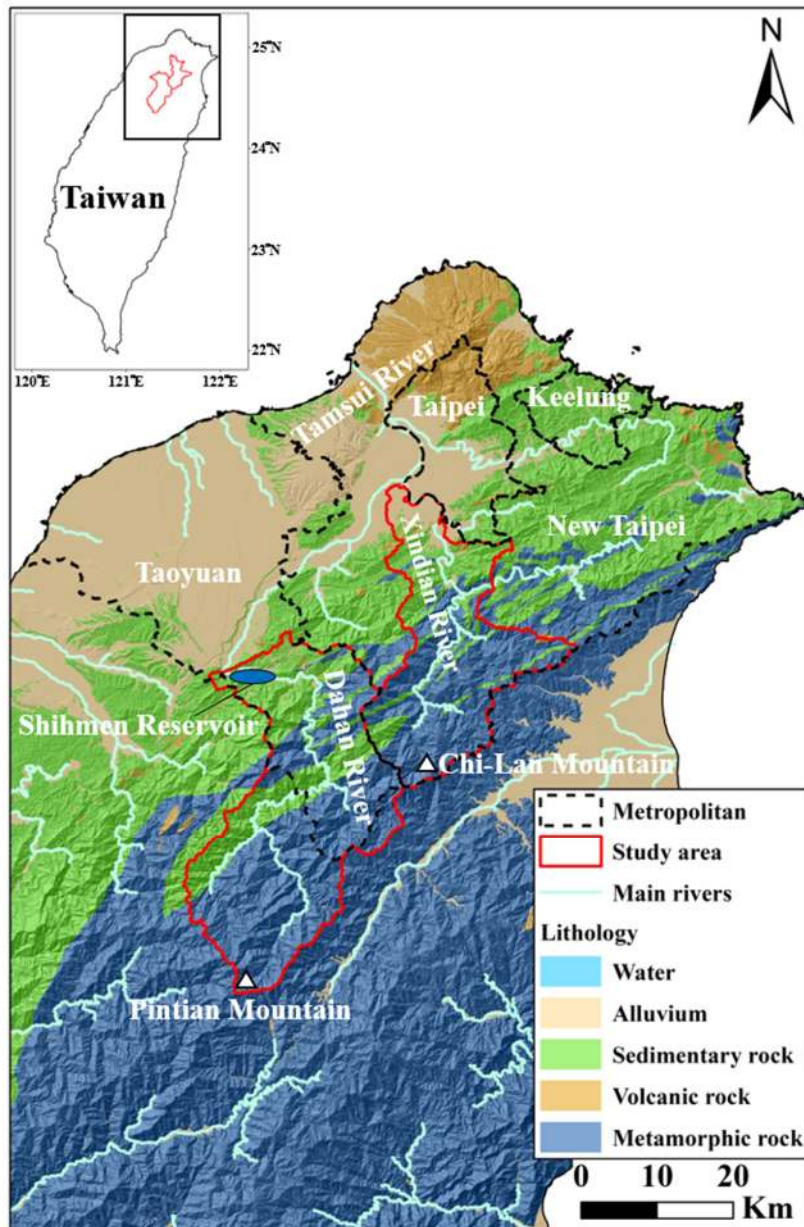

Figure 2. Geographic location of the study area.

Each climate change scenario will have different weights on the empirical models for estimating landslide-area characteristics. The most important factor is the future SST change in each scenario (Figure 1), affecting the circulation of the ocean and the atmosphere and leading to different rainfall patterns. Then the changes of cumulative rainfall and peak rainfall intensity will be different in different

regions, which will greatly affect the local landslide-area characteristics. Chen et al. [16] estimated the impact of climate change on landslide-area characteristics for the two catchments but only used single scenarios, m01 and c0, for the base period and the end of the 21st century, respectively. As we mentioned in Section 2, climate change is so full of uncertainty that there are many possible scenarios for the present and the future. The ensemble method is one of the most effective approaches for dealing with many possible climate change scenarios. In this method, the data from all scenarios are combined to obtain the most reliable predictions for the present and future [31–33]. For example, there is a total of 10 typhoons in a single scenario so that if the top 10% typhoons according to a certain rainfall condition are taken, there will be only one typhoon. On the other hand, using the ensemble method to consider all scenarios together, the number of typhoons is assumed to be 100, and the top 10% typhoons will have as many as 10 times the number of typhoons (10 typhoons). In this study, we used two scenarios (m00 and m01) for the base period and four scenarios (c0, c1, c2, and c3) for the end of the 21st century. Based on the cumulative rainfall for the Shihmen Reservoir catchment and peak rainfall intensity for the Xindian River catchment during typhoon events, we chose the top 15% typhoons for each scenario and for the ensembles (Table 1). We then estimated the landslide-area characteristics during those typhoons and evaluated the effects of climate change.

4. Results

Tables 2 and 3 show the results of average rainfall conditions (cumulative rainfall and peak rainfall intensity) and estimated landslide-area characteristics of the two catchments during top typhoons under different climate change scenarios for the base period and the end of the 21st century. For the base period in the Shihmen Reservoir catchment, the highest cumulative rainfall of 1183.69 mm appeared in the scenario of m00, resulting in 896 landslides, with a maximum landslide area of 9.49×10^5 m^2, a total landslide area of 6.30 km^2, and a landslide-area ratio of 0.81%. In the Xindian River catchment, the highest peak rainfall intensity of 52.85 mm/h appeared in the scenario of m01, resulting in 181 landslides, with a maximum landslide area of 1.18×10^5 m^2, a total landslide area of 0.71 km^2, and a landslide-area ratio of 0.15%. In addition, for the end of the 21st century in the Shihmen Reservoir catchment, the highest cumulative rainfall of 1327.07 mm appeared in the scenario of c3, resulting in 996 landslides, with a maximum landslide area of 1.08×10^6 m^2, a total landslide area of 6.97 km^2, and a landslide-area ratio of 0.89%. In the Xindian River catchment, the highest peak rainfall intensity of 71.17 mm/h appeared in the scenario of c0, resulting in 291 landslides, with a maximum landslide area of 1.90×10^5 m^2, a total landslide area of 1.14 km^2, and a landslide-area ratio of 0.24%. Details of each typhoon can be found on the website (https://drive.google.com/file/d/1CYkCYBOvWK3Jm4gyaJBNf3i5uenO8U_h/view?usp=sharing).

Table 2. The range of average rainfall conditions and possible landslide characteristics in the Shihmen Reservoir catchment during top 15% typhoon events. "()" is the average value of a scenario.

Scenario		Cumulative Rainfall (mm)	Peak Rainfall Intensity (mm/h)	Number of Landslides	Maximum Landslide Area (m^2)	Total Landslide Area (km^2)	Landslide-Area Ratio (%)
Base period	m00	250.20–1183.69 (522.37)	20.27–53.70 (35.19)	245–896 (435)	8.87×10^4–9.49×10^5 (3.40×10^5)	1.91–6.30 (3.19)	0.25–0.81 (0.41)
	m01	222.30–749.31 (432.08)	18.20–58.76 (36.30)	226–593 (372)	6.29×10^4–5.49×10^5 (2.56×10^5)	1.78–4.26 (2.77)	0.23–0.55 (0.36)
End of 21st century	c0	365.92–1097.48 (605.22)	32.76–72.01 (54.80)	326–836 (493)	1.95×10^5–8.70×10^5 (4.11×10^5)	2.46–5.89 (3.58)	0.32–0.76 (0.46)
	c1	528.53–726.81 (636.71)	24.85–61.51 (46.33)	439–578 (514.67)	3.45×10^5–5.28×10^5 (4.45×10^5)	3.22–4.15 (3.73)	0.41–0.53 (0.48)
	c2	374.73–597.31 (487.72)	26.28–60.20 (45.23)	332–487 (410.91)	2.03×10^5–4.09×10^5 (3.08×10^5)	2.50–3.54 (3.03)	0.32–0.46 (0.39)
	c3	353.68–1327.07 (685.82)	36.09–93.29 (54.74)	318–996 (549)	1.84×10^5–1.08×10^6 (4.90×10^5)	2.40–6.97 (3.96)	0.31–0.89 (0.51)

Table 3. The range of average rainfall conditions and possible landslide characteristics in the Xindian River catchment during top 15% typhoon events. "()" is the average value of a scenario.

Scenario		Cumulative Rainfall (mm)	Peak Rainfall Intensity (mm/h)	Number of Landslides	Maximum Landslide Area (m^2)	Total Landslide Area (km^2)	Landslide-Area Ratio (%)
Base period	m00	122.42–700.96 (371.45)	22.92–46.73 (32.19)	0–144 (56)	8.85×10^2–9.43×10^4 (3.72×10^4)	0.06–0.56 (0.24)	0.00–0.12 (0.05)
	m01	146.29–553.02 (303.62)	25.09–52.85 (33.68)	13–181 (65)	9.40×10^3–1.18×10^5 (4.31×10^4)	0.05–0.71 (0.26)	0.02–0.15 (0.05)
End of 21st century	c0	211.56–685.89 (395.58)	33.13–71.17 (46.11)	62–291 (140)	4.10×10^4–1.90×10^5 (9.09×10^4)	0.24–1.14 (0.55)	0.05–0.24 (0.12)
	c1	298.61–670.32 (483.30)	34.09–56.57 (41.55)	68–203 (113)	4.47×10^4–1.33×10^5 (7.40×10^4)	0.26–0.80 (0.44)	0.06–0.17 (0.09)
	c2	121.50–556.64 (318.87)	31.54–45.04 (39.05)	52–134 (98)	3.47×10^4–8.77×10^4 (6.42×10^4)	0.20–0.52 (0.38)	0.04–0.11 (0.08)
	c3	73.46–1358.02 (508.37)	36.01–54.53 (44.30)	79–191 (129.29)	5.23×10^4–1.25×10^5 (8.49×10^4)	0.31–0.75 (0.51)	0.06–0.16 (0.11)

5. Discussion

According to the results of landslide-area characteristic estimation, we counted the landslide-area characteristics for the top 10% of typhoon events of each scenario and ensemble. Figure 3 shows the maximum, minimum, and mean values, and the 95% confidence intervals of statistical results of landslide-area characteristics for each scenario and ensemble. The maximum value represents the most severe condition of landslides triggered by the typhoon. The 95% confidence interval represents the range of statistical uncertainty from the mean value. It appears that the range of maximum and minimum values and the range of the 95% confidence interval differed greatly among the different scenarios. Sometimes the range of values was very small, but the uncertainty was very large (e.g., the c1 scenario for the Shihmen Reservoir catchment), which means that the simulation by the scenario can only catch a small part of the possibility in current and future periods, and the results are still questionable (Figure 3a–d). On the other hand, sometimes the range of uncertainty was small, but the range of values was also small (e.g., the c2 scenario for the Xindian River catchment). The uncertainty of simulation from this kind of scenario is quite low, but the possible most severe condition cannot be grasped (Figure 3e–h). This may be due to the fact that model characteristics of those models, grouped in the c2 scenario, only reflect a narrow possibility of future climate, resulting in a very low climate variability. The SST of c2 scenario was moderate among the groups (Figure 1), so that no severe rainfall events could be observed in future climate simulations, which may also be one of the reasons. Generally speaking, the ensemble approach not only minimized the uncertainty (i.e., narrowing the 95% confidence interval), but also identified the worst case from the simulation [34,35]. From the results of the ensembles for the top 10% typhoons during the base period and the end of the 21st century, on average, the total landslide area, landslide-area ratio, maximum landslide area, and number of landslide in the Shihmen Reservoir catchment will increase from 3.53 ± 0.60 to 4.02 ± 0.58 km^2, 0.46 ± 0.08 to 0.52 ± 0.07%, $(4.06 \pm 1.18) \times 10^5$ to $(5.03 \pm 1.13) \times 10^5$ m^2, and 485 ± 89 to 559 ± 86, while those in the Xindian River catchment will increase from 0.31 ± 0.09 to 0.57 ± 0.11 km^2, 0.07 ± 0.02 to 0.12 ± 0.02%, $(5.33 \pm 1.54) \times 10^4$ to $(9.57 \pm 1.74) \times 10^4$ m^2, and 81 ± 24 to 146 ± 27, respectively.

Here we further separated typhoon events into the top 5%, 5%–10%, and 10%–15% to confirm possible changes in landslide-area characteristics from the base period to the end of the 21st century. Previous studies in Taiwan often used m01 and c0 as simulation scenarios for the base period and the end of the 21st century, and they explored the impact of climate change [16,36,37]. Figure 4 shows the landslide-area characteristics of the top 5%, 5%–10%, and 10%–15% typhoons during the base period and the end of the 21st century in the Shihmen Reservoir catchment and the Xindian River catchment simulated only with the m01 and c0 scenarios. If we only look at the average values of landslide-area characteristics (red and blue lines in Figure 4), there are indeed some differences between the base period and the end of the 21st century. We can use these differences to assess the change ratios of landslide-area characteristics affected by climate change in the future. However, if we consider the uncertainty of the simulations, the 95% confidence intervals at the base period and the end of the 21st century almost overlap (red and blue areas in Figure 4), which means that this result cannot really explain the difference between the present and the future. Chen et al. [16] also pointed out that the future is full of uncertainty, for changes in human activities and the efficiency of carbon reduction will bring additional effects, which may lead to different possibilities. More climate change scenarios must be incorporated, and the ensemble method must be employed to achieve more reliable results.
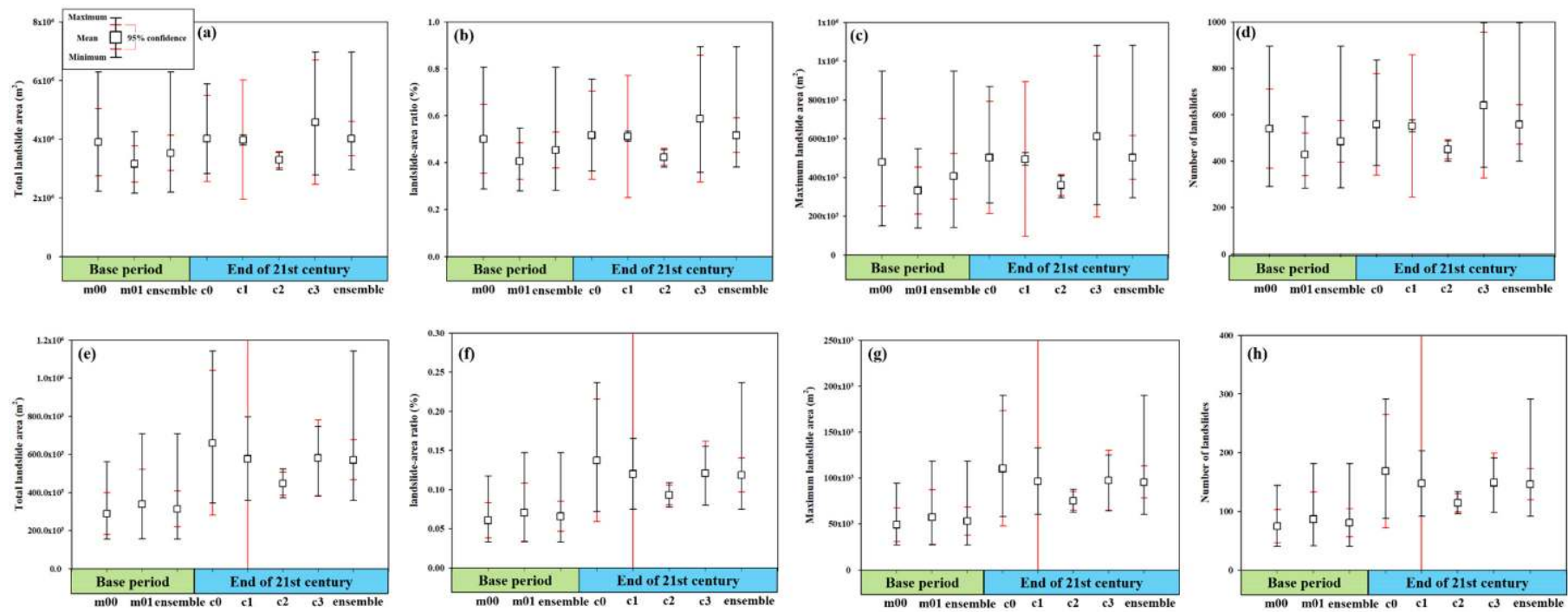
Figure 3. Statistics of landslide-area characteristics for the top 10% typhoons of each scenario and ensemble during the base period and the end of the 21st century. (**a**–**d**) are for the Shihmen Reservoir catchment and (**e**–**h**) are for the Xindian River catchment.
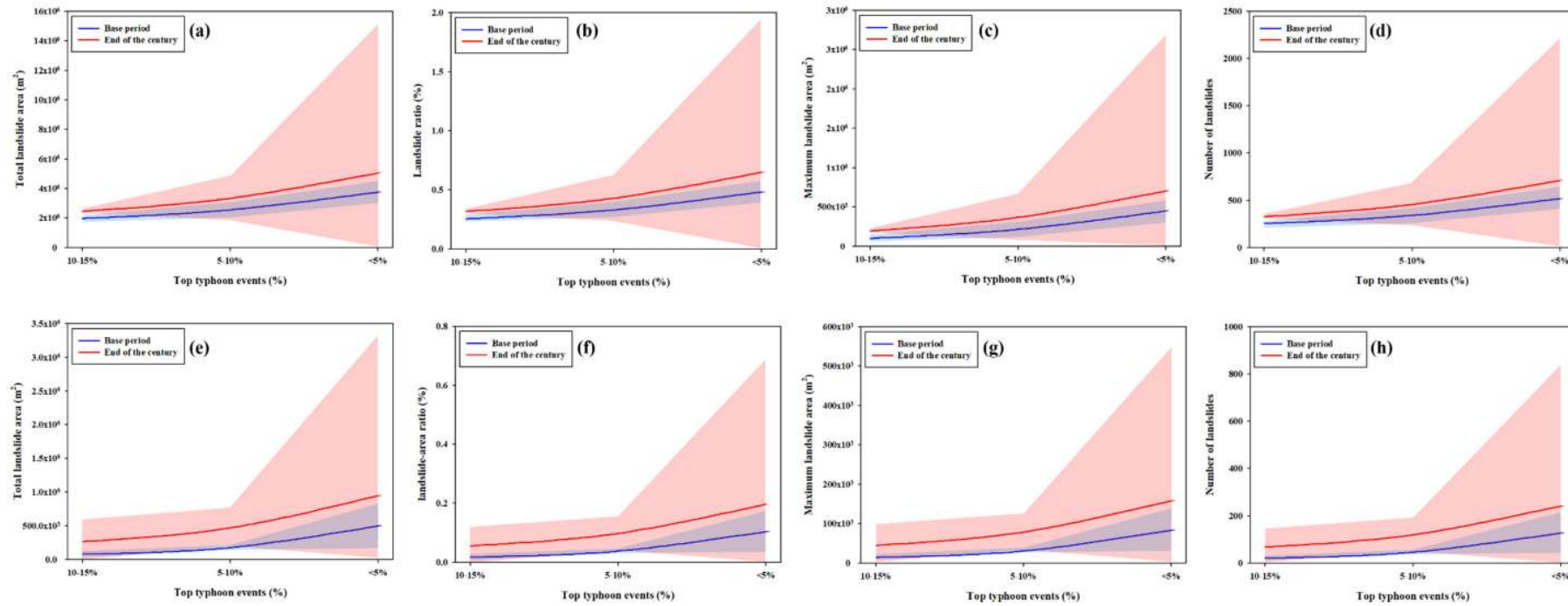
Figure 4. Landslide-area characteristics of the top 5%, 5%–10%, and 10%–15% typhoons during the base period and the end of the 21st century simulated only with the m01 and c0 scenarios. (**a**–**d**) are for the Shihmen Reservoir catchment and (**e**–**h**) are for the Xindian River catchment. Red and blue lines are mean values of landslide-area characteristics, with 95% confidence intervals in red and blue areas, respectively.

Figure 5 shows the landslide-area characteristics of the top 5%, 5%–10%, and 10%–15% typhoons during the base period and the end of the 21st century in the Shihmen Reservoir catchment and the Xindian River catchment simulated by scenario ensembles. It is very clear that the ensemble approach successfully distinguished the difference between the base period and the end of the 21st century in the average values of landslide-area characteristics and 95% confidence intervals. From the top 10%–15% to the top 5% typhoon events, the uncertainty of landslide-area characteristics showed an increasing trend, indicating that the more extreme the event, the greater the uncertainty [38]. In the Shihmen Reservoir catchment, the 95% confidence intervals of the base period and the end of the 21st century still partially overlapped at the top 5% typhoons. In contrast, in the Xindian River catchment, they were completely separated. Chen et al. [16] indicated that under the impact of climate change, both the landslide severity and the landslide frequency will increase more in the Xindian River catchment than in the Shihmen Reservoir catchment, owing to the increased possibility of the occurrence of a strong typhoon and the higher rainfall intensity during a typhoon event [20–22]. This is why the changes in the landslide-area characteristics of the Xindian River catchment during extreme typhoon events under climate change are more significant than those of the Shihmen Reservoir catchment. Based on the robust ensemble approach, the landslide-area ratios in the Shihmen Reservoir catchment triggered by the top 10%–15%, 5%–10%, and 5% typhoons during the base period will be $0.27 \pm 0.01\%$, $0.34 \pm 0.04\%$, and $0.57 \pm 0.09\%$, while those in the last quarter of the 21st century will be $0.35 \pm 0.02\%$, $0.42 \pm 0.02\%$, and $0.62 \pm 0.12\%$. In the Xindian River catchment, the landslide-area ratios triggered by the top 10%–15%, 5%–10%, and 5% typhoons during the base period will be $0.02 \pm 0.01\%$, $0.04 \pm 0.01\%$, and $0.09 \pm 0.03\%$, while those in the last quarter of the 21st century will be $0.06 \pm 0.00\%$, $0.09 \pm 0.01\%$, and $0.16 \pm 0.03\%$. The landslide-area ratios triggered by medium- and high-level typhoons (top 5%–15%) will increase by 24%–29% and 125%–200% from the base period to the end of the 21st century in the Shihmen Reservoir catchment and the Xindian River catchment, respectively, while those triggered by extreme-level typhoons (top 5%) will increase by 8% and 77%, respectively (Table 4). Under climate change, the landslide severity in the Xindian River catchment will increase more than that in the Shihmen Reservoir catchment, which indicates that rainfall intensity will increase more than cumulative rainfall. Changes in the SST under climate change will mainly result in more concentrated rainfall. Therefore, in the future with the change of landslide characteristics, special attention needs to be paid to the problem of serious surface erosion.

In the climate change research, changes in related hydrological hazards have traditionally been analyzed with climate change simulated by a specific scenario [16,36,37]. However, the future is full of uncertainties that changes in human activities and the efficiency of reducing carbon emissions will bring additional impacts, which may result in different possibilities. In addition, a single model may be affected by the model characteristics, leading to more biased results. Climate scientists have therefore come up with many models and scenarios to simulate various future possibilities. There is no exact declaration as to which result is the true future, but the ensemble method can discuss all possibilities together and effectively reduce uncertainty. This study used all available climate change scenarios in Taiwan and applied the ensemble method, providing the most reliable estimation on future landslide characteristics for the study area. This study can also contribute to other regions of Taiwan or areas other than Taiwan as a reference approach for related hazard assessment under climate change. Even though this study reduced the uncertainty in assessing the impact of climate change with the ensemble approach, the uncertainty of landslide-area characteristics caused by extreme typhoon events (top 5%) was still slightly high. Therefore, more climate change scenarios should be included to improve the accuracy of assessing climate change impacts. Recently, the Coupled Model Intercomparison Project 6 (CMIP6) provided new possibilities for climate change scenarios and should be considered in future works [39]. Moreover, landslide characteristics can be evaluated not only by empirical methods, but also by other methods, such as numerical simulations [40,41] and statistical methods [42–44], which can be used to integrate the results of all methodologies to obtain more reliable results.
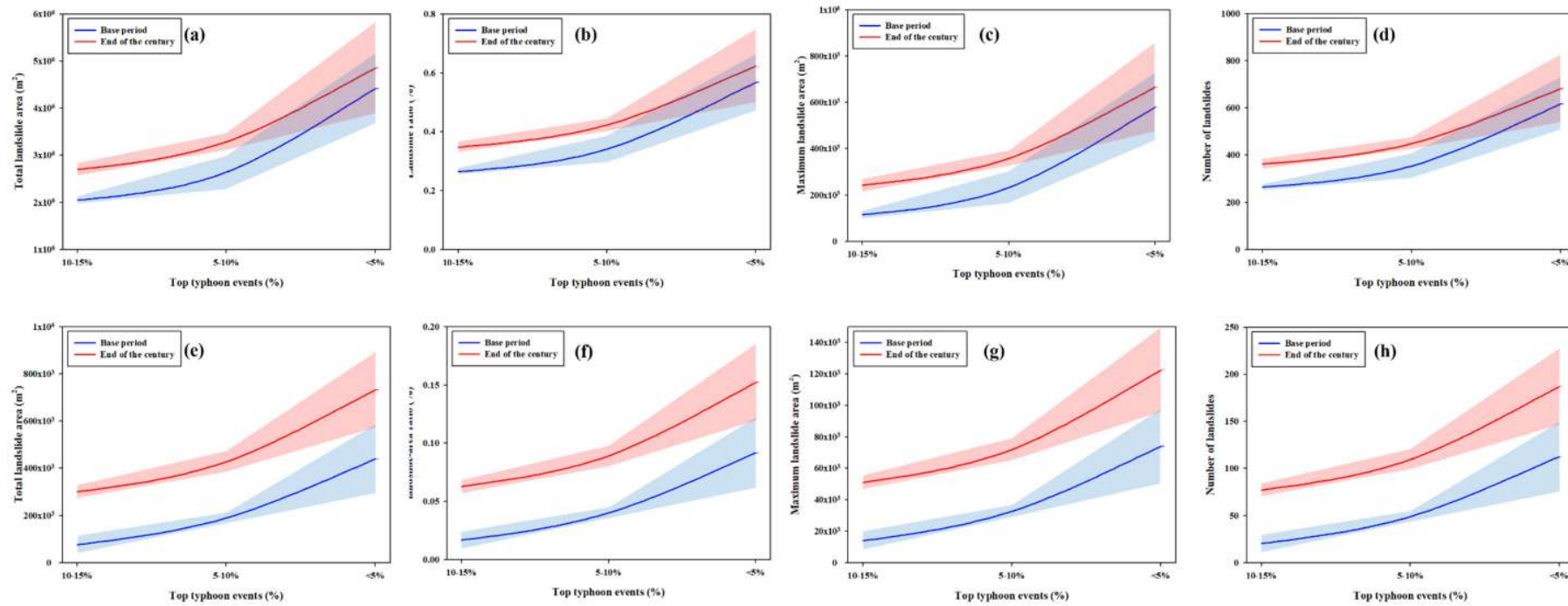
Figure 5. Landslide-area characteristics of the top 5%, 5%–10%, and 10%–15% typhoons during the base period and the end of the 21st century simulated with scenario ensembles. (**a**–**d**) are for the Shihmen Reservoir catchment and (**e**–**h**) are for the Xindian River catchment. Red and blue lines are mean values of landslide-area characteristics, with 95% confidence intervals in red and blue areas, respectively.

Table 4. Landslide-area ratio triggered by the top typhoons and its percentage increase during the base period and the last quarter of the 21st century in the Shihmen Reservoir catchment and the Xindian River catchment.

Top Typhoons	Shihmen Reservoir Catchment			Xindian River Catchment		
	Base Period	End of 21st Century	Percentage Increase	Base Period	End of 21st Century	Percentage Increase
5%	0.57 ± 0.09%	0.62 ± 0.12%	8%	0.09 ± 0.03%	0.16 ± 0.03%	77%
5–10%	0.34 ± 0.04%	0.42 ± 0.02%	24%	0.04 ± 0.01%	0.09 ± 0.01%	125%
10–15%	0.27 ± 0.01%	0.35 ± 0.02%	29%	0.02 ± 0.01%	0.06 ± 0.00%	200%

6. Conclusions

This study used two and four climate change scenarios for the base period and the end of the 21st century, respectively, to analyze the impact of climate change on landslide-area characteristics with the ensemble approach. In total, 166 and 169 typhoons were simulated for the base period and the last quarter of the 21st century, respectively, and rainfall conditions of the two catchments in northern Taiwan for each of the top 15% typhoon events (*n* = 24 and 25) were analyzed. According to the empirical relationship between rainfall conditions and landslide-area characteristics proposed by a previous study, the landslide-area characteristics triggered by each top 15% typhoon were calculated. Comparing the landslide-area characteristics triggered by the top 10% typhoons between every single scenario and the ensembles, the ensemble approach not only minimized the uncertainty, but also identified the most severe case from the simulation. This study further separated typhoon events into the top 5%, 5%–10%, and 10%–15% to confirm possible changes in landslide-area characteristics under climate change. We noticed that the uncertainty of the base period and the end of the 21st century almost overlapped if only a single scenario was used, indicating that the difference between the present and the future could not really be explained. The ensemble approach successfully distinguished the differences between the base period and the end of the 21st century in the average values of the landslide-area characteristics and 95% confidence intervals. Based on the robust ensemble approach, the landslide magnitudes triggered by medium- and high-level typhoons (top 5%–15%) will increase by 24%–29% and 125%–200% under climate change in the Shihmen Reservoir catchment and the Xindian River catchment, respectively. In contrast, those triggered by extreme-level typhoons (top 5%) will increase by 8% and 77%, respectively.

Author Contributions: Conceptualization: C.-W.C., Y.-C.C. and Y.-S.T.; Data curation: Y.-M.C., J.-J.L., H.-C.L. and C.-T.C.; Formal analysis: Y.-M.C.; Methodology: Y.-C.C. and Y.-S.T.; Project administration: C.-W.C.; Supervision: C.-W.C.; Writing, original draft: Y.-M.C. and C.-W.C.; Writing, review & editing: J.-J.L., H.-C.L. and C.-T.C. All authors have read and agreed to the published version of the manuscript.

References

1. IPCC. *Climate Change 2007: The Physical Science Basis*; Summary for Policymakers; Contribution of Working Group I to the Fourth Assessment Report; The Intergovernmental Panel on Climate Change: Geneva, Switzerland, 2007.
2. IPCC. *Climate Change 2013: The Physical Science Basis*; Summary for Policymakers; Contribution of Working Group I to the Fifth Assessment Report; The Intergovernmental Panel on Climate Change: Geneva, Switzerland, 2013.
3. Crozier, M.J. Deciphering the effect of climate change on landslide activity: A review. *Geomorphology* **2010**, *124*, 260–267. [CrossRef]
4. Kao, S.C.; Ganguly, A.R. Intensity, duration, and frequency of precipitation extremes under 21st-century warming scenarios. *J. Geophys. Res.-Atmos.* **2011**, *116*. [CrossRef]
5. Jibson, R.W.; Keefer, D.K. Statistical analysis of factors affecting landslide distribution in the New Madrid seismic zone, Tennessee and Kentucky. *Eng. Geol.* **1989**, *27*, 509–542. [CrossRef]
6. Nagarajan, R.; Roy, A.; Kumar, R.V.; Mukherjee, A.; Khire, M.V. Landslide hazard susceptibility mapping based on terrain and climatic factors for tropical monsoon regions. *B Eng. Geol. Environ.* **2000**, *58*, 275–287. [CrossRef]
7. Collison, A.; Wade, S.; Griffiths, J.; Dehn, M. Modelling the impact of predicted climate change on landslide frequency and magnitude in SE England. *Eng. Geol.* **2000**, *55*, 205–218. [CrossRef]

8.　Soldati, M.; Corsini, A.; Pasuto, A. Landslides and climate change in the Italian Dolomites since the Late glacial. *Catena* **2004**, *55*, 141–161. [CrossRef]

9.　Jakob, M.; Lambert, S. Climate change effects on landslides along the southwest coast of British Columbia. *Geomorphology* **2009**, *107*, 275–284. [CrossRef]

10.　Melchiorre, C.; Frattini, P. Modelling probability of rainfall-induced shallow landslides in a changing climate, Otta, Central Norway. *Clim. Chang.* **2012**, *113*, 413–436. [CrossRef]

11.　Turkington, T.; Remaître, A.; Ettema, J.; Hussin, H.; van Westen, C. Assessing debris flow activity in a changing climate. *Clim. Chang.* **2016**, *137*, 293–305. [CrossRef]

12.　Chiang, S.H.; Chang, K.T. The potential impact of climate change on typhoon-triggered landslides in Taiwan, 2010–2099. *Geomorphology* **2011**, *133*, 143–151. [CrossRef]

13.　Timbal, B.; Jones, D.A. Future projections of winter rainfall in southeast Australia using a statistical downscaling technique. *Clim. Chang.* **2008**, *86*, 165–187. [CrossRef]

14.　Timm, O.; Diaz, H.F. Synoptic-statistical approach to regional downscaling of IPCC twenty-first-century climate projections: Seasonal rainfall over the Hawaiian Islands. *J. Clim.* **2009**, *22*, 4261–4280. [CrossRef]

15.　Sunyer, M.A.; Madsen, H.; Ang, P.H. A comparison of different regional climate models and statistical downscaling methods for extreme rainfall estimation under climate change. *Atmos. Res.* **2012**, *103*, 119–128. [CrossRef]

16.　Chen, C.W.; Tung, Y.S.; Liou, J.J.; Li, H.C.; Cheng, C.T.; Chen, Y.M.; Oguchi, T. Assessing landslide characteristics in a changing climate in northern Taiwan. *Catena* **2019**, *175*, 263–277. [CrossRef]

17.　Chen, C.W.; Saito, H.; Oguchi, T. Rainfall intensity–duration conditions for mass movements in Taiwan. *Prog. Earth Planet. Sci.* **2015**, *2*, 1–13. [CrossRef]

18.　Wu, C.H.; Chen, S.C. Determining landslide susceptibility in Central Taiwan from rainfall and six site factors using the analytical hierarchy process method. *Geomorphology* **2009**, *112*, 190–204. [CrossRef]

19.　Wu, C.H.; Chen, S.C.; Chou, H.T. Geomorphologic characteristics of catastrophic landslides during typhoon Morakot in the Kaoping Watershed, Taiwan. *Eng. Geol.* **2011**, *123*, 13–21. [CrossRef]

20.　Emanuel, K. Increasing destructiveness of tropical cyclones over the past 30 years. *Nature* **2005**, *436*, 686–688. [CrossRef]

21.　Webster, P.J.; Holland, G.J.; Curry, J.A.; Chang, H.R. Changes in tropical cyclone number, duration, and intensity in a warming environment. *Science* **2005**, *309*, 1844–1846. [CrossRef]

22.　Tu, J.Y.; Chou, C.; Chu, P.S. The abrupt shift of typhoon activity in the vicinity of Taiwan and its association with western North Pacific–East Asian climate change. *J. Clim.* **2009**, *22*, 3617–3628. [CrossRef]

23.　Hsu, H.H.; Chou, C.; Wu, Y.C.; Lu, M.M.; Chen, C.T.; Chen, Y.M. *Climate Change in Taiwan: Scientific Report 2011 (Summary)*; National Science Council: Taipei, Taiwan, 2011.

24.　Mizuta, R.; Arakawa, O.; Ose, T.; Kusunoki, S.; Endo, H.; Kitoh, A. Classification of CMIP5 future climate responses by the tropical sea surface temperature changes. *SOLA* **2014**, *10*, 167–171. [CrossRef]

25.　Wilks, D.S. *Statistical Methods in the Atmospheric Sciences*; Academic press: Oxford, UK, 2011; Volume 100, p. 704.

26.　Roble, R.G.; Ridley, E.C. A thermosphere-ionosphere-mesosphere-electrodynamics general circulation model (TIME-GCM): Equinox solar cycle minimum simulations (30–500 km). *Geophys. Res. Lett.* **1994**, *21*, 417–420. [CrossRef]

27.　Johns, T.C.; Carnell, R.E.; Crossley, J.F.; Gregory, J.M.; Mitchell, J.F.; Senior, C.A.; Tett, S.F.B.; Wood, R.A. The second Hadley Centre coupled ocean-atmosphere GCM: Model description, spinup and validation. *Clim. Dyn.* **1997**, *13*, 103–134. [CrossRef]

28.　Mizuta, R.; Yoshimura, H.; Murakami, H.; Matsueda, M.; Endo, H.; Ose, T.; Kamiguchi, K.; Hosaka, M.; Sugi, M.; Yukimoto, S.; et al. Climate simulations using MRI-AGCM3.2 with 20-km grid. *J. Meteorol. Soc. Jpn.* **2012**, *90*, 233–258. [CrossRef]

29.　Murakami, H.; Wang, Y.; Yoshimura, H.; Mizuta, R.; Sugi, M.; Shindo, E.; Adachi, Y.; Yukimoto, S.; Hosaka, M.; Kusunoki, S.; et al. Future changes in tropical cyclone activity projected by the new high-resolution MRI-AGCM. *J. Clim.* **2012**, *25*, 3237–3260. [CrossRef]

30.　Murakami, H.; Hsu, P.C.; Arakawa, O.; Li, T. Influence of model biases on projected future changes in tropical cyclone frequency of occurrence. *J. Clim.* **2014**, *27*, 2159–2181. [CrossRef]

31. Giorgi, F.; Mearns, L.O. Calculation of average, uncertainty range, and reliability of regional climate changes from AOGCM simulations via the reliability ensemble averaging (REA) method. *J. Clim.* **2002**, *15*, 1141–1158. [CrossRef]

32. Ruosteenoja, K.; Tuomenvirta, H.; Jylhä, K. GCM-based regional temperature and precipitation change estimates for Europe under four SRES scenarios applying a super-ensemble pattern-scaling method. *Clim. Chang.* **2007**, *81*, 193–208. [CrossRef]

33. Kling, H.; Fuchs, M.; Paulin, M. Runoff conditions in the upper Danube basin under an ensemble of climate change scenarios. *J. Hydrol.* **2012**, *424*, 264–277. [CrossRef]

34. Müller, W.A.; Appenzeller, C.; Doblas-Reyes, F.J.; Liniger, M.A. A debiased ranked probability skill score to evaluate probabilistic ensemble forecasts with small ensemble sizes. *J. Clim.* **2005**, *18*, 1513–1523. [CrossRef]

35. Tiwari, M.K.; Chatterjee, C. Uncertainty assessment and ensemble flood forecasting using bootstrap based artificial neural networks (BANNs). *J. Hydrol.* **2010**, *382*, 20–33. [CrossRef]

36. Wu, T.; Li, H.C.; Wei, S.P.; Chen, W.B.; Chen, Y.M.; Su, Y.F.; Liu, J.J.; Shih, H.J. A comprehensive disaster impact assessment of extreme rainfall events under climate change: A case study in Zheng-wen river basin, Taiwan. *Environ. Earth Sci.* **2016**, *75*, 597. [CrossRef]

37. Chao, Y.C.; Chen, C.W.; Li, H.C.; Chen, Y.M. Riverbed Migrations in Western Taiwan under Climate Change. *Water* **2018**, *10*, 1631. [CrossRef]

38. Fischer, E.M.; Knutti, R. Anthropogenic contribution to global occurrence of heavy-precipitation and high-temperature extremes. *Nat. Clim. Chang.* **2015**, *5*, 560–564. [CrossRef]

39. Eyring, V.; Bony, S.; Meehl, G.A.; Senior, C.A.; Stevens, B.; Stouffer, R.J.; Taylor, K.E. Overview of the Coupled Model Intercomparison Project Phase 6 (CMIP6) experimental design and organization. *Geosci. Model Dev.* **2016**, *9*, 1937–1985. [CrossRef]

40. Hungr, O.; McDougall, S. Two numerical models for landslide dynamic analysis. *Comput. Geosci.* **2009**, *35*, 978–992. [CrossRef]

41. Katz, O.; Morgan, J.K.; Aharonov, E.; Dugan, B. Controls on the size and geometry of landslides: Insights from discrete element numerical simulations. *Geomorphology* **2014**, *220*, 104–113. [CrossRef]

42. Van Westen, C.J.; Rengers, N.; Soeters, R. Use of geomorphological information in indirect landslide susceptibility assessment. *Nat. Hazards* **2003**, *30*, 399–419. [CrossRef]

43. Bai, S.B.; Wang, J.; Lü, G.N.; Zhou, P.G.; Hou, S.S.; Xu, S.N. GIS-based logistic regression for landslide susceptibility mapping of the Zhongxian segment in the Three Gorges area, China. *Geomorphology* **2010**, *115*, 23–31. [CrossRef]

44. Borgatti, L.; Soldati, M. Landslides as a geomorphological proxy for climate change: A record from the Dolomites (northern Italy). *Geomorphology* **2010**, *120*, 56–64. [CrossRef]